BRNO UNIVERSITY OF TECHNOLOGY
VYSOKÉ UČENÍ TECHNICKÉ V BRNĚ

FACULTY OF ELECTRICAL ENGINEERING AND COMMUNICATION
FAKULTA ELEKTROTECHNIKY
A KOMUNIKAČNÍCH TECHNOLOGIÍ

DEPARTMENT OF RADIO ELECTRONICS
ÚSTAV RADIOELEKTRONIKY

OPTIMAL INTENSITY DISTRIBUTION IN A LASER BEAM FOR FSO COMMUNICATIONS
OPTIMÁLNÍ ROZLOŽENÍ OPTICKÉ INTENZITY V LASEROVÉM SVAZKU PRO FSO KOMUNIKACE

SHORT VERSION OF PHD THESIS
ZKRÁCENÁ VERZE PHD THESIS

AUTHOR — **Ing. Peter Barcík**
AUTOR PRÁCE

SUPERVISOR — **prof. Ing. Otakar Wilfert, CSc.**
ŠKOLITEL

BRNO 2016

Keywords: Top-hat beam, Gaussian beam, scintillation index, atmospheric turbulence, refraction beam shaper, aspheric optical elements.

Klíčová slova: Top-hat zväzok, Gaussovský zväzok, index scintilácie, atmosferické turbulencie, refrakčný tvarovač zväzku, asférické optické prvky.

Rukopis disertační práce je uložen na:
Ústav Radioelektroniky
Fakulta elektrotechniky a komunikačních technologií
Vysoké učení technické v Brně
Technická 3082/12
616 00 Brno

Contents

INTRODUCTION

For about 30 years, Free-Space Optical (FSO) systems have been gaining a specific place in the wireless technology area. The FSO system is line of sight technology which is designed to transmit information with a modulated infrared laser beam from one point to another in free space. On the other side of the link the information is received and demodulated. The application of these systems is advantageous for high speed point to point communication links in an urban area where the last mile problem arises. Another application of FSO system is in space-to-ground links. FSO technology brings advantages, e.g. high bandwidth, a license free band, no electromagnetic interference, and quick deployment. High directivity of the laser beam ensures more security of conveyed information but also brings a more difficult alignment procedure in comparison with the Radio Frequency (RF) system. The most serious drawback of FSO systems is their dependence on the state of the atmosphere causing deterioration of the FSO system's availability. Hence, the FSO system can be regarded as an atmospheric sensor. The performance of the FSO terminals and transmission of the optical wave through the atmosphere are affected mainly by atmospheric turbulence, fog, snow, wind, rain, background radiation, etc.

Constituent particles of the atmosphere cause absorption and scattering. These phenomena have the most serious impact on the FSO link availability. A power margin of the link working in foggy conditions has to be set appropriately to overcome fog attenuation and thus reduce the probability of fade. Another atmospheric effect which has an essential impact on the performance of FSO systems is atmospheric turbulence. Atmospheric turbulence leads to fluctuation of the optical intensity in the plane of the receiving aperture.

This unwanted effect caused by atmospheric turbulence can be mitigated by a number of techniques. Basic techniques for mitigating received power fluctuations include aperture averaging and spatial diversity [1, 2, 3, 4, 5] in transmission as well as in reception. Another widely discussed technique is the usage of random optical beams. It is already known that the application of different beam shapes (Flattened Gaussian (FG) beams, Bessel-Gaussian beams, etc.) increases the reliability and availability of FSO systems. The scintillation index of Bessel-Gaussian beams propagating in turbulent media was studied theoretically in [6, 7]. The application of nondiffracting beams with different degrees of coherence in FSO systems was experimentally tested in [8].

In this thesis we are focusing only on usage of FG beams in FSO systems. The propagation of the FG beam in a turbulent atmosphere has been extensively studied theoretically in [9, 10, 11]. The usage of FG beams is advantageous from a practical point of view. The generation of Airy beams, Bessel-Gaussian beams, etc.

requires special optical devices such as an axicon or spatial light modulator. On the other hand, generating an FG beam is relatively inexpensive with optical components such as a diffuser, refraction optics and lenslet array. This thesis will discuss the propagation of FG beams in a turbulent atmosphere. We simulated propagation of the Gaussian and FG beam in a weak and moderate atmospheric turbulent medium. The thesis also discusses the selection of appropriate FG beam width in FSO transmitters and aperture averaging effect in FSO receivers.

Photonic components usually used for optical fiber communication are nowadays utilized in fully optical FSO links. It means that the light is not converted from optical to electrical domain, but the received light is directly coupled into the optical fiber. The received light can be advantageously amplified by an EDFA and filtered by a fiber filter. In the last chapter the concept of the fully photonic receiver and transmitter is discussed.

1 OBJECTIVES OF THE THESIS

The dissertation thesis is focused on analysing the distribution of optical intensity within a radiated laser beam at the transmitter and receiver plane which is affected by propagation through free space as well as through the atmosphere. The aim of the thesis is to determine the optimal intensity distribution of a laser beam at the transmitter plane which is minimally affected by turbulence during the propagation process. As a consequence, the scintillation index should be reduced. The most important objectives of the thesis are as follows:

- The first aim is to create a simulation program for studying the propagation of an arbitrary optical wave through the atmosphere. The program will be able to simulate different strengths of turbulences with a specified turbulence power spectrum.

- Based on the findings of the theoretical analysis and simulations, the second aim is to design a laser beam transmitter with the ability to shape a Gaussian beam to a top-hat beam.

- The third aim is to design and practically validate properties of a fully photonic link which will be able to transmit an optical signal without the need to convert it into the electrical domain. Data gathered during experimental testing will be compared with theoretical assumptions.

2 FLATTENED-GAUSSIAN BEAM

For a mathematical expression of the circularly symmetrical FG beam at the transmitter plane (TXA) located in $z = 0$, approximation proposed by Bagini et al. [12] can be used

$$U_{TXA}(\mathbf{s}, z = 0) = A \exp\left(-\frac{(N+1)\, s^2}{w_0^2}\right) \sum_{m=0}^{N} \frac{1}{m!} \left(\frac{\sqrt{N+1}s}{w_0}\right)^{2m}. \qquad (2.1)$$

The parameter A is amplitude of the field distribution, $\mathbf{s}$ is transverse vector at TXA plane, s is radial distance from the optical axis, w_0 is beam half-width at TXA and $N \geq 0$ is flatness order [13]. With increasing N, the FG profile becomes flatter (Fig. 2.1). If the parameter N is equal to zero, the FG beam turns into a Gaussian beam. We used this expression in order to determine intensity distribution U_{TXA} at the transmitter plane.

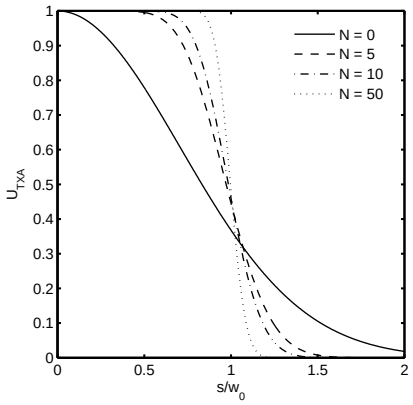

Fig. 2.1: FG beam for various N parameters as a function of radial distance normalized with beam half-width

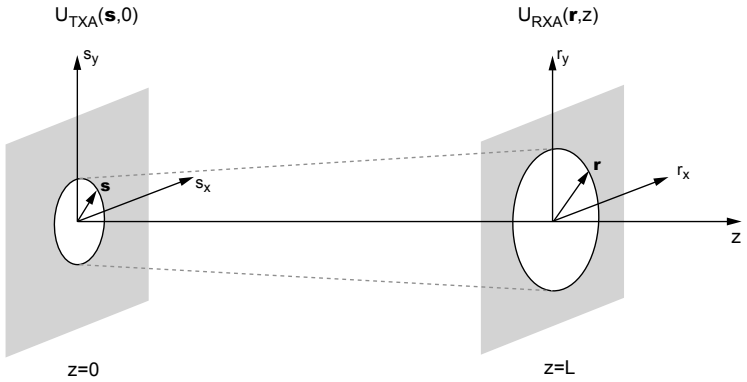

Fig. 2.2: Propagation scheme

The intensity distribution at the receiver plane U_{RXA} can be determined by using the Huygens-Fresnel diffraction integral as follows

$$U_{RXA}(\mathbf{r}, z) = \frac{-ik}{2\pi z} \exp(ikz) \int_{-\infty}^{\infty} \int_{-\infty}^{\infty} U_{TXA}(\mathbf{s}, 0) \exp\left(\frac{ik}{2z} |\mathbf{s} - \mathbf{r}|^2\right) ds^2, \tag{2.2}$$

where z is the distance between the TXA and RXA plane, $\mathbf{r}$ is transverse vector at the RXA plane, k is wave number, $U_{TXA}(\mathbf{s}, 0)$ is the intensity distribution and $\mathbf{s}$ is transverse vector at the TXA plane. The scheme of propagation is depicted in Fig. 2.2. In order to simulate the propagation of the FG beam in a vacuum, it is convenient to rewrite Eq. 2.2 as a convolution of the field at the TXA plane with the free-space amplitude spread function [14]

$$U_{RXA}(\mathbf{r}, z) = U_{TXA}(\mathbf{s}, 0) * \left(\frac{-ik}{2\pi z} \exp\left(ikz + \frac{ik}{2z} |\mathbf{s} - \mathbf{r}|\right)\right). \tag{2.3}$$

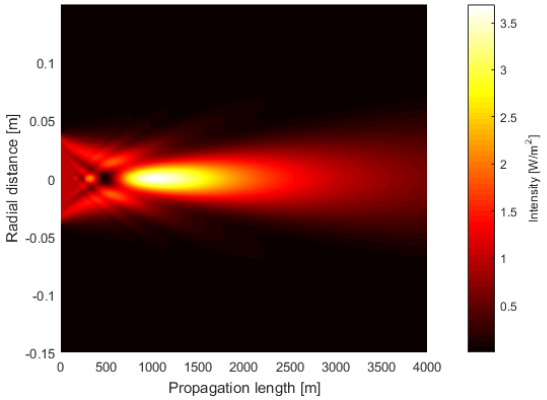

Fig. 2.3: Longitudinal intensity distribution of the FG beam for vacuum propagation

We performed the simulation of Eq. 2.3 to evaluate the intensity distribution across the propagation length. The FG beam half-width was set to $w_0 = 40\,\text{mm}$, flatness parameter N=10 and wavelength 1550 nm. In Fig. 2.3, it can be seen that the FG beam with high flatness parameter N acts like a plane wave diffracted on a circular aperture with a radius equal to the FG beam half-width. As the beam is propagated, the transverse optical intensity distribution changes and the middle part of the beam reaches its minimum. From this minimum point, two Fresnel zones are observed exactly at the TXA plane. The Fresnel zone, in our case, can be defined as follows

$$N_{Fresnel} = \frac{w_0^2}{L\lambda}, \tag{2.4}$$

where $N_{Fresnel}$ is the number of Fresnel zone and L is the distance between the plane with minimum and the TXA plane. If the FG beam is further propagated, its shape turns into a Gaussian or Airy function.

2.1 Simulation of Flattened Gaussian beam propagation

The numerical simulation was used to simulate propagation of the FG beam through weak and moderate atmospheric turbulences (Fig. 2.4).

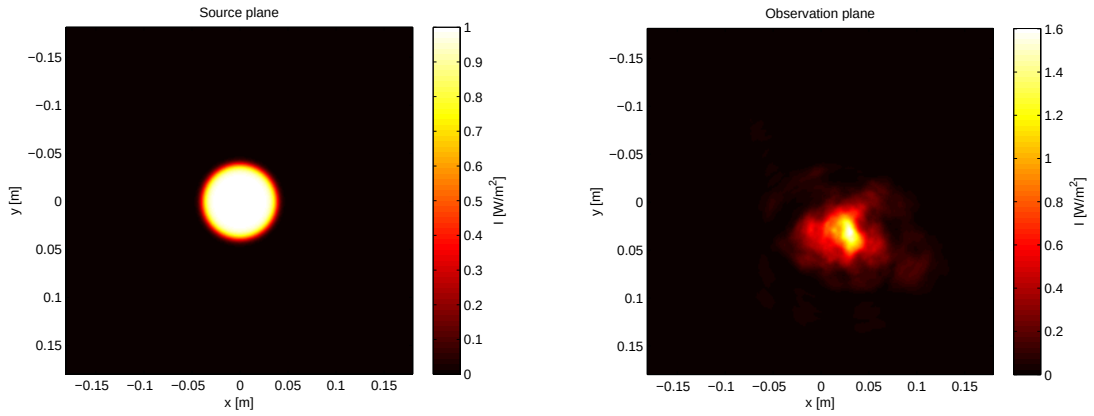

(a) (b)

Fig. 2.4: Initial top-hat beam (a) and irradiance resulting from turbulence propagation (b) for $C_n^2 = 10^{-14}\, m^{-2/3}$

The initial wavefront is propagated through regions of turbulences which are represented by random phase screens [14]. As a result, a variation in irradiance across the wavefront is observed. The on-axis scintillation index was calculated from 500 random runs.

The simulation was carried out for an FG beam with beam radius 10 mm and 40 mm at TXA plane and for flatness parameter $N = 0$ (Gaussian beam) and $N = 10$ (FG beam).

From Fig. 2.5, a very interesting fact is notable. The FG beam with radius 10 mm at TXA plane has almost the same on-axis scintillation index as the Gaussian beam. However, this fact is not valid for beam radius 40 mm at TXA plane (Fig. 2.6), where the on-axis scintillation index is lower in comparison with a Gaussian beam for reasonable link lengths. Another interesting fact is that there is a peak of the on-axis scintillation index around 600 m. The peak is located at the place in which two Fresnel zones on TXA plane are observed. The height of the peak is

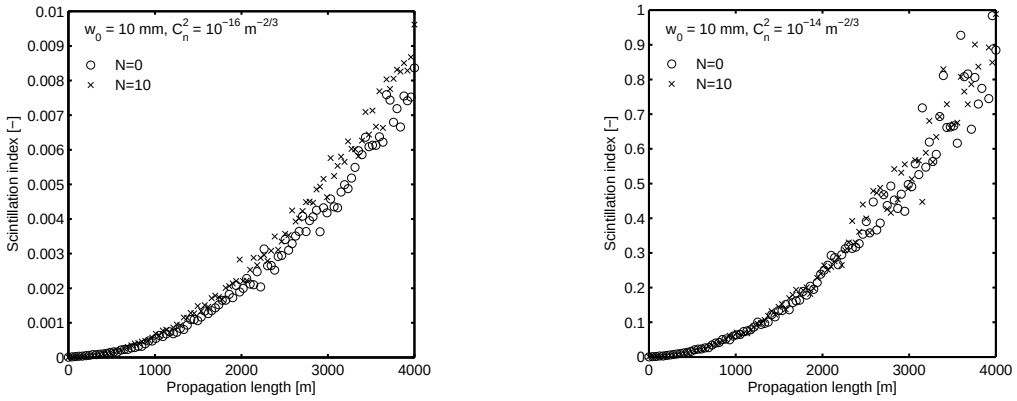

Fig. 2.5: Simulated on-axis scintillation index as a function of propagation length for the FG beam with radius 10 mm at TXA plane

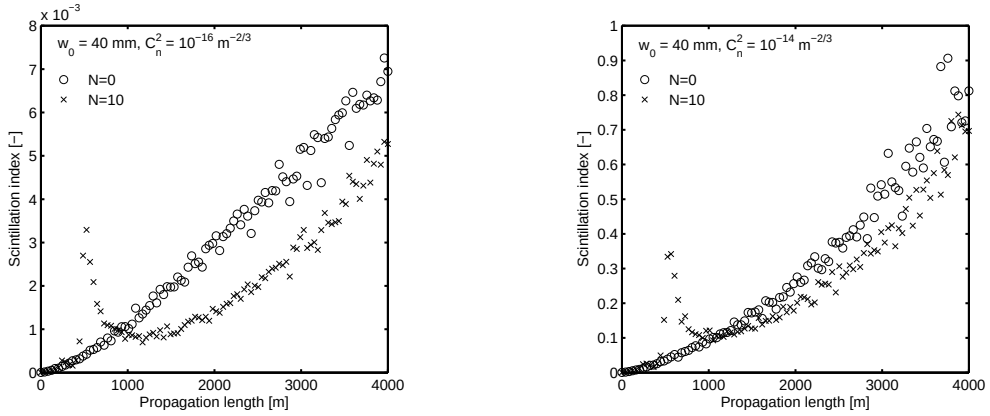

Fig. 2.6: Simulated on-axis scintillation index as a function of propagation length for the FG beam with radius 40 mm at TXA plane

dependent on the order of the flatness parameter of the FG beam. The higher the value of the flatness parameter N is, the higher the scintillation peak is observed.

Simulation data for FG beam on-axis scintillation as a function of beam radius at TXA plane for two N parameters are depicted in Fig. 2.7. One can see that the size of the FG beam at the TXA plane plays an important role in the scintillation analysis. Note, that the on-axis scintillation for N=0 is firstly almost constant and then increasing slightly for beam radius above 0.05 m. On the other hand, on-axis scintillation for N=10 is slightly decreasing and then reaches minimum around the radius 0.05 m. If the radius of the beam is further increased the scintillation starts to increase rapidly and then falls to the same value as for N=0. Therefore, we can estimate the optimal radius of the FG beam, where scintillation for the propagation length 4 km is minimal. The optimal radius for weak and moderate turbulence

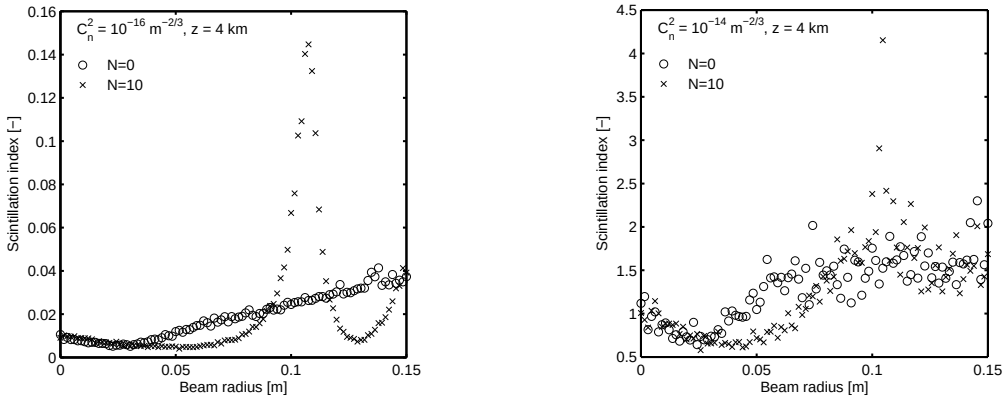

Fig. 2.7: Simulated scintillation index for the FG beam as a function of beam radius at the TXA

regime should be slightly bigger than the radius of the first Fresnel zone, which is also defined by $\sqrt{L/k}$.

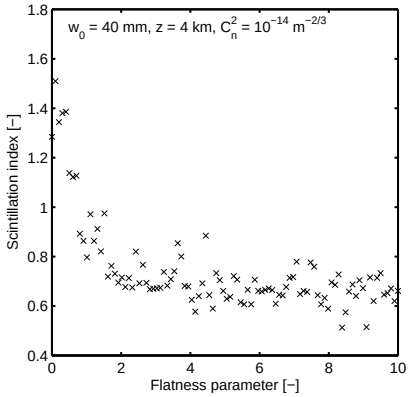

Fig. 2.8: Simulated scintillation index for the FG beam as a function of flatness parameter N

For the sake of maximal reduction of scintillation, we plot the scintillation index as a function of flatness parameter N (Fig. 2.8). It is obvious that the scintillation index is decreasing with increasing parameter N. Thus the N parameter should be high enough.

2.2 Aperture averaging

In this section we analysed effect of the aperture averaging on the scintillation for the FG beam with flatness parameter N=10. The simulation was carried out for circular receiving aperture with radius up to 150 mm. The increasing radius of a

receiving aperture, for given beam divergence, wavelength and propagation distance, has noticeable impact on power scintillation reduction, as shown in Fig. 2.9. For the receiving aperture with radius bigger than 50 mm the scintillation peak is diminished completely. As was stated above, the scintillation reduction is quantified by parameter called the aperture averaging factor. The aperture averaging factor as a function of radius of the receiving aperture for three different beam half-widths at the TXA plane is depicted in Fig. 2.10. With increasing radius of the receiving

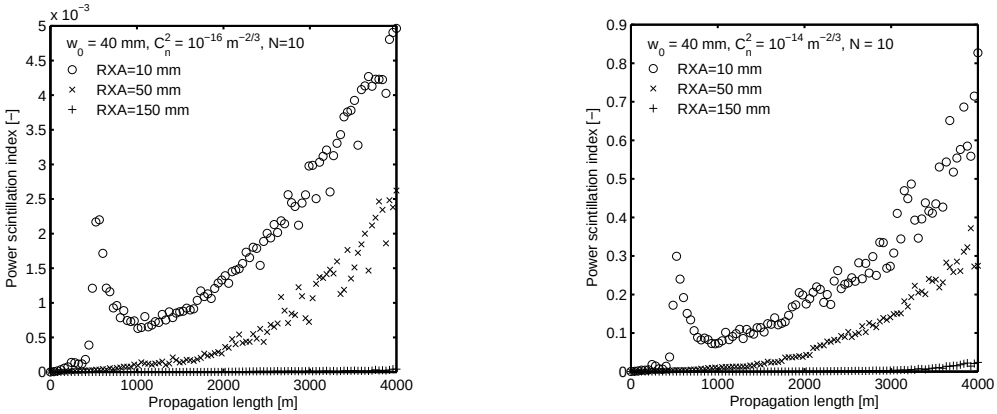

Fig. 2.9: Power scintillation index as a function of propagation length for different radius of receiving aperture

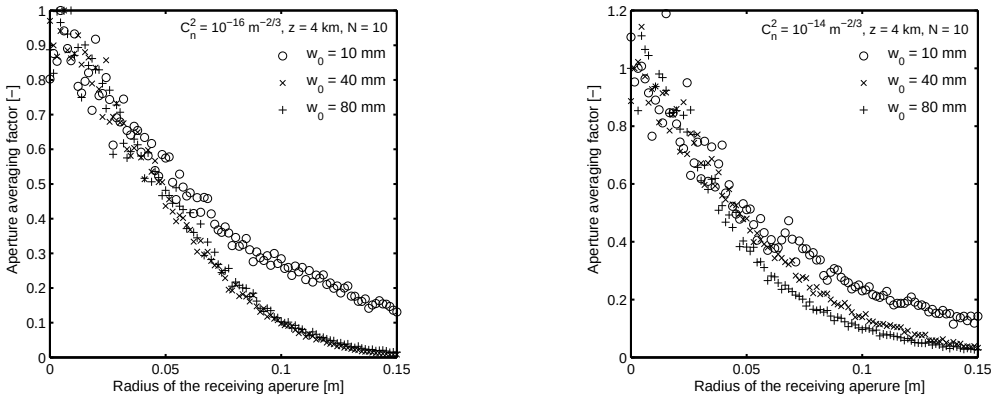

Fig. 2.10: Aperture averaging factor as a function of radius of the receiving aperture

aperture the aperture averaging factor decreases and thus the scintillation of the received power decreases. It can be seen that value of aperture averaging factor depends on beam half-width at the TXA and beam divergence. The scintillation of the power is averaged out more for the FG beam with half-width 40 mm in comparison with half-width 10 mm. In case of using receiving aperture with radius above 0.15 m, aperture averaging factor is almost the same for FG beam with half-width 40 mm

and 80 mm. The previous statements are valid for weak and moderate turbulence regime.

3 BEAM SHAPER FOR FREE SPACE OPTICAL COMMUNICATION TRANSMITTER

After the results presented in the previous chapter, it can be stated that the optimal distribution of optical intensity within a laser beam at the TXA is uniform. However, coherent optical sources like lasers and laser diodes emit a light whose intensity profile can be approximated by a Gaussian function. So the intensity distribution has to be transformed into a uniform function. There exist several transformation methods to obtain the uniform optical intensity distribution at the output plane of beam shaping optics. Some of the methods are appropriate for laser beams with a high degree of coherence, and other methods are applicable to non coherent optical sources. The transformation techniques can also be divided according to the measure of conversion losses. One group of shaping techniques is known as field mapping. It is suitable for coherent optical sources [15]. The other methods, which are cost effective and also applicable for non coherent sources, are beam integrators [15].

3.1 Optical fiber as a beam shaper

In this section we are dealing with problem how to achieve uniform distribution of the optical intensity at the receiver plane. One of the possibility is using of optical fiber as a transmitting fiber. The intensity of light emanating from three different fibers was studied. For the comparison the single mode fiber is also included. Thereafter we analysed multi-mode gradient index fiber and multimode step index fiber with large core diameter. The technical parameters of the fibers are summarized in Tab. 3.1.

In Fig. 3.1 is depicted intensity distribution emanating from the single mode fiber. Only one fundamental mode is propagated and intensity distribution has Gaussian character with peak at the center. The optical intensity distribution of multi-mode gradient index fiber is depicted in Fig. 3.2. It is clear that there are dozens of modes propagated inside the fiber. In order to excite as many modes as possible the fiber was scrambled with mode scrambler. The mode scrambler has to be used because fiber was only 2 meters long and single mode laser was used as a light source.

Tab. 3.1: Parameters of the optical fibers

	Fiber 1	Fiber 2	Fiber 3
Type	Single - mode	Multi - mode gradient index	Multi - mode step index
Core diameter [μm]	10	62.5	1000
Core material	Fused silica	Fused silica	Fused silica
Numerical aperture (NA)	0.130	0.275	0.220
Attenuation @ 1550 nm [dB/km]	0.18	0.6	400
Wavelength range [nm]	980 – 1550	800 – 1600	350 – 2500

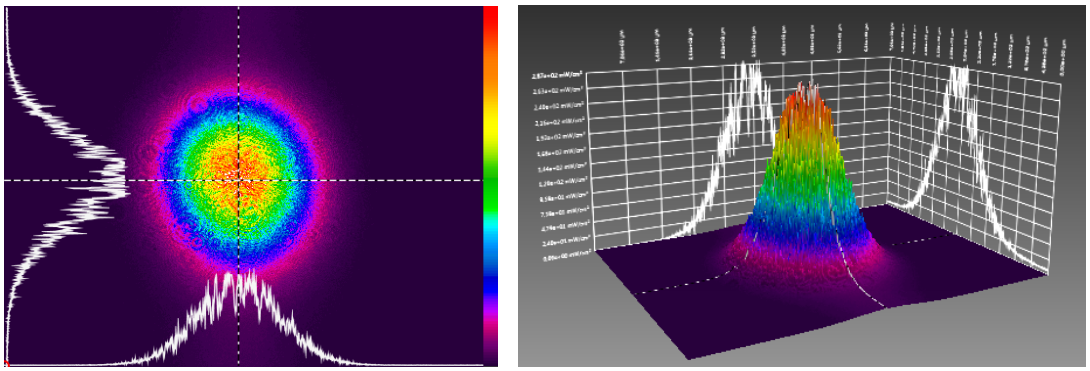

(a) (b)

Fig. 3.1: Optical intensity distribution of the single mode fiber

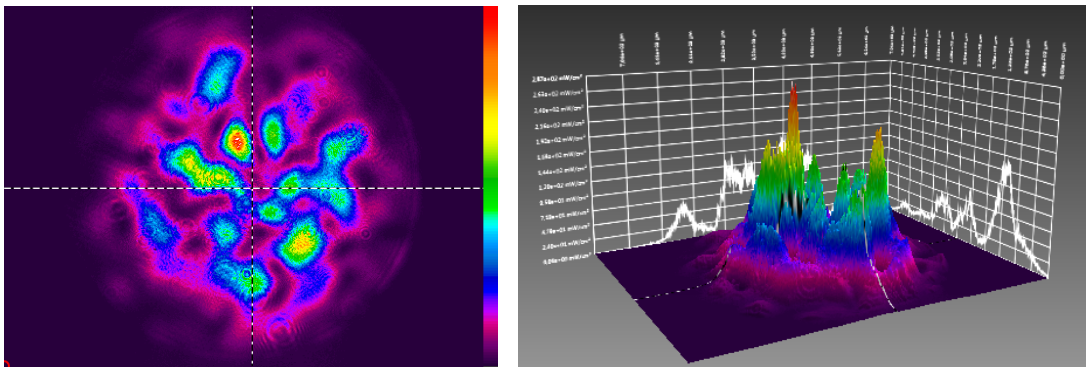

(a) (b)

Fig. 3.2: Optical intensity distribution of the multimode fiber

The third fiber is multi mode step index fiber with large core diameter. The

diameter of the core is 1000 µm. A large core fibers are usually used as a spectrometer probes. Due to high attenuation of the fibers, they are used for short distance communication and car communication inside a car. Even the lenght of the fiber was only 2 meters all modes were excited without any mode scrambler. When the intensity distribution was depicted, very interesting fact was observed. The intensity distribution is created with million of modes and the envelope of this modes looks like top–hat beam (see Fig. 3.3). The short fiber can be used in the transmitter as a shaping element. As a result one get more uniform distribution of the optical intensity at the RXA plane.

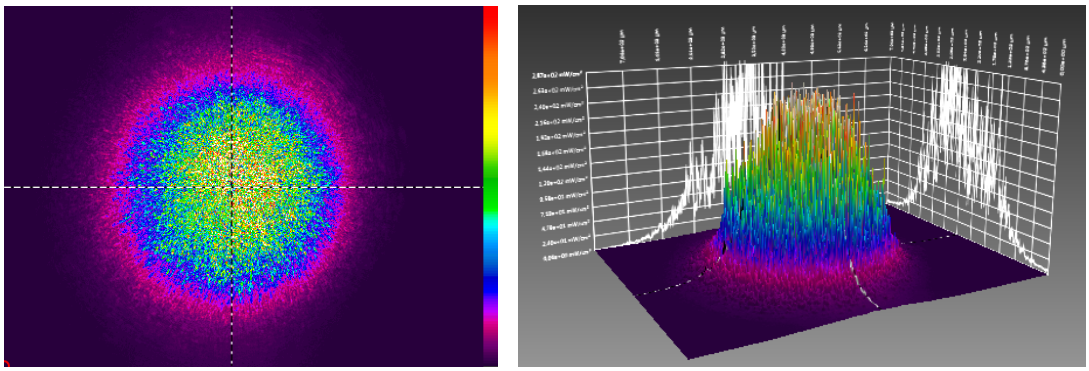

(a) (b)

Fig. 3.3: Optical intensity distribution of the plastic fiber

Another feature of the large core fiber is that it acts like a phase diffuser and emanating light became partially coherent. It was shown in many publications that partially coherent beam is less affected by atmospheric turbulences [16, 17].

4 FULLY PHOTONIC LINK

The perspective technology, which can increase resistance of the FSO link to atmospheric effects, is concept of the fully photonic FSO terminals [18, 19]. The outdoor unit of the fully photonic FSO terminal consists of only passive optical components. Active components like lasers, photodiodes, fiber amplifiers, fiber couplers and supply parts are placed in the indoor unit, which does not suffer on weather changes.

4.1 Transmitter with large core optical fiber

The purpose of the Fully Photonic Transmitter (FPT) is to create a transmitted optical beam by an optical fiber irradiating the transmitting lens (achromatic doublet

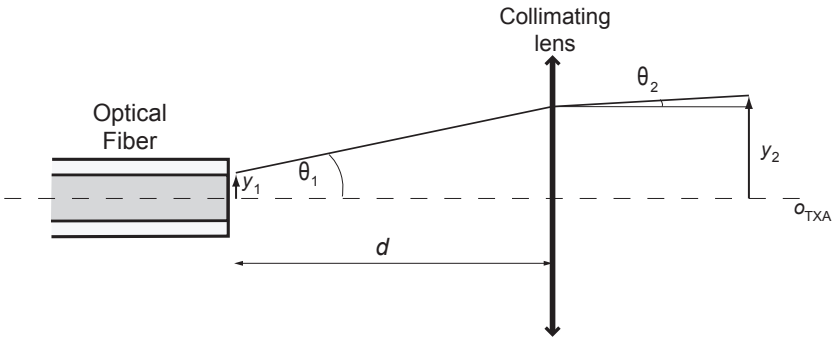

Fig. 4.1: Design of the transmitter

lens). If the multimode fiber (plastic or glass) is used as a final fiber, the optical intensity distribution in the transmitted beam will generate a so-called "top-hat" beam [19], which is more resistant to the negative effects of atmospheric turbulence in comparison with the standard Gaussian beam.

An optical fiber AVANTES FC-IR1000-2-FC/PC with core diameter 1 mm and numerical aperture NA = 0.22 was used as the transmitting fiber in our model. The attenuation of the fiber 2 meters long is approximately 0.8 dB. For modeling the FPT function, it is sufficient to apply the matrix optics methods.

The translation matrix describing the free space propagation of the optical ray through the distance d between the output aperture of the optical fiber and principal plane of the transmitting optical system (achromatic doublet lens) is expressed as follows [20]

$$\mathbf{M_T} = \begin{bmatrix} 1 & d \\ 0 & 1 \end{bmatrix}. \tag{4.1}$$

The transmitting optical system (Fig. 4.1) is modeled as a thin ideal lens with focal length f_{TXA}. Propagation of the optical ray through this lens is described by the refraction matrix $\mathbf{M_R}$

$$\mathbf{M_R} = \begin{bmatrix} 1 & 0 \\ -\frac{1}{f_{\mathrm{TXA}}} & 1 \end{bmatrix}. \tag{4.2}$$

The resulting transfer matrix, between the output aperture of the optical fiber and output plane of the achromatic doublet lens, could be expressed by transfer matrix (4.1) and refraction matrix (4.2). The output ray parameters at the output of the collimating lens (transmitting aperture) are given by (Fig. 4.1)

$$\begin{bmatrix} y_2 \\ \theta_2 \end{bmatrix} = \mathbf{M_R}\,\mathbf{M_T} \begin{bmatrix} y_1 \\ \theta_1 \end{bmatrix}. \tag{4.3}$$

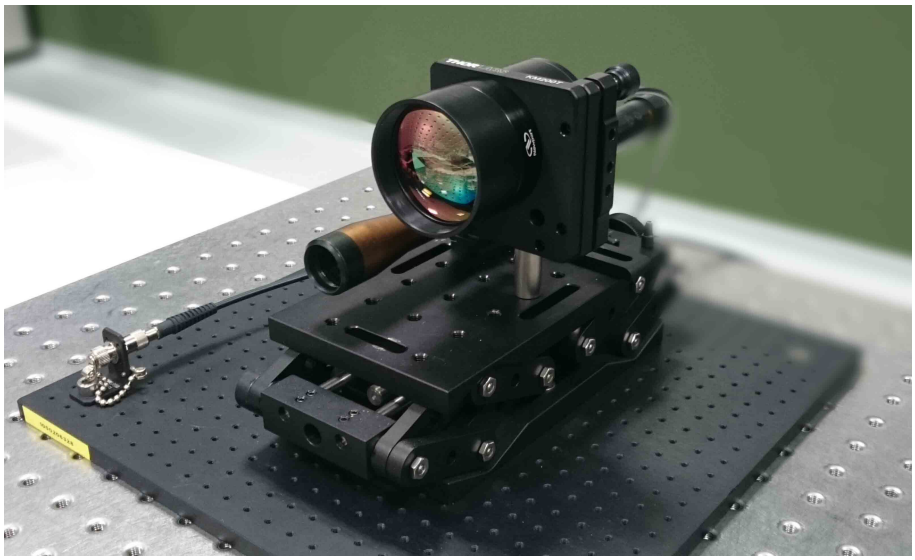

Fig. 4.2: Transmitter with plastic optical fiber.

Therefore, parameters of the transmitted ray (y_j and θ_j, $j = 1, 2$) can characterize the parameters of the transmitted beam: distance of the ray from the optical axis y_j corresponds to beam radius, and angle between the ray and optical axis θ_j agree with beam divergence. After substituting matrices (4.1) and (4.2) into equation (4.3) we get the relations for beam radius y_2 and beam divergence θ_2

$$y_2 = y_1 + d\,\theta_1, \tag{4.4}$$

$$\theta_2 = -\frac{y_1}{f_{\mathrm{TXA}}} + \theta_1 \left(\frac{d}{f_{\mathrm{TXA}}} - 1 \right). \tag{4.5}$$

An achromatic doublet lens THORLABS AC508-075-C with focal length $f_{\mathrm{TXA}} = 75\,\mathrm{mm}$ and diameter $D_{\mathrm{TXA}} = 50\,\mathrm{mm}$, which is suitable for the transmitting optical system, was chosen as the collimating lens from commercially available lenses. The lens is coated for C-band 1050 - 1700 nm. After substituting the angle θ_1, which is given by the numerical aperture of the transmitting fiber and core radius of the transmitting fiber y_1, into (4.4) and (4.5) we get the divergence of the transmitted optical beam 1 mrad.

From the energetic point of view it is need to check whether the NA of the fiber is lower than NA of the transmitting lens. Numerical aperture of the transmitting lens can be calculated as follows

$$NA_{\mathrm{lens}} \approx \frac{1}{2\,f\#} \tag{4.6}$$

where $f\#$ is f number of the lens given by ratio of the focal lenght f and diameter of the lens D. After the substitution of the lens parameters into the 4.6 we get

$NA_{\text{lens}} = 0.33$. The numerical aperture of the transmitting lens is bigger than numerical aperture of the fiber, therefore the energetic condition is fulfilled.

4.2 Fully photonic receiver

The most challenging part of the fully photonic terminal is to design the fully photonic receiver (FPR). The purpose of the FPR is to focus the received optical power to the core of a receiving optical fiber with diameter of only few micrometers. In order to estimate the coupling efficiency in laboratory condition it is needed to design the testbed (Fig. 4.5). In the section, we numerically design the testbed for measuring the coupling efficiency of the FPR. The testbed consists of the Testing Transmitter (TT) and FPR under test. The numerical model is based on transformation of the Gaussian beam through optical system described by ray transfer matrix. The step by step design process is added and finally the coupling efficiency of the FPR is theoretically estimated for single-mode fiber.

The FPR concept is shown in Fig. 4.5. The optical wave captured by the Cassegrain telescope is collimated using an aspheric collimating lens and guided to the GRIN lens, which is connected to an receiving optical fiber at its output. The outgoing collimated optical wave from the aspherical lens is ensured by tuning the focal length f_{tel} of the Cassegrain telescope (Fig. 4.3).

Fig. 4.3: Prototype of the FPR.

This section presents considerations and requirements on the FPR design used for optical beam coupling from free-space to an optical fiber at $\lambda = 1550$ nm.

The FPR model was created using matrix optics methods, which assumes beam propagation in Gaussian paraxial space (rays are propagated near the optical axis

with a small deviation from the direction of the axis).

In order to get the whole ray transfer matrix of the system, the Cassegrain telescope is modelled as a thin positive lens, whose refraction matrix

$$\mathbf{M_{1'}} = \begin{bmatrix} 1 & 0 \\ {}^{-1}/_{f_{tel}} & 1 \end{bmatrix} \tag{4.7}$$

is situated at the principal plane of the receiving lens. The ray transfer between the principal plane of the receiving lens and the principal plane of the aspherical lens is expressed by the translation matrix

$$\mathbf{M_{1'2'}} = \begin{bmatrix} 1 & f_{tel} + f_A \\ 0 & 1 \end{bmatrix}. \tag{4.8}$$

For the refraction matrix of the aspherical lens situated at the principal plane of the lens, it is possible to write

$$\mathbf{M_{2'3'}} = \begin{bmatrix} 1 & 0 \\ {}^{-1}/_{f_A} & 1 \end{bmatrix}. \tag{4.9}$$

The distance between the principal plane of the aspherical lens and input aperture of the GRIN element is given by the translation matrix

$$\mathbf{M_{3'4'}} = \begin{bmatrix} 1 & d_3 \\ 0 & 1 \end{bmatrix}. \tag{4.10}$$

The GRIN lens refraction matrix can be expressed as follows [21]

$$\mathbf{M_{5'6'}} = \begin{bmatrix} \cos(g\, l_g) & \frac{1}{g\, n_g} \sin(g\, l_g) \\ g\, n_g \sin(g\, l_g) & \cos(g\, l_g) \end{bmatrix}, \tag{4.11}$$

where g is gradient constant, l_g is length and n_g is refraction index at the center of the GRIN lens. For the maximum coupling efficiency the fiber is placed at the working distance of the GRIN lens. Working distance d_w is represented by the following translation matrix

$$\mathbf{M_{7'8'}} = \begin{bmatrix} 1 & d_w \\ 0 & 1 \end{bmatrix}. \tag{4.12}$$

The ray transfer matrix of the complete receiving optical system $\mathbf{M_R}$ is given by multiplying all the elementary matrices in the correct order

$$\mathbf{M_R} = \mathbf{M_{7'8'}} \cdot \mathbf{M_{5'6'}} \cdot \mathbf{M_{3'4'}} \cdot \mathbf{M_{2'3'}} \cdot \mathbf{M_{1'2'}} \cdot \mathbf{M_{1'}}. \tag{4.13}$$

After rearrangement we obtain

$$\mathbf{M_R} = \begin{bmatrix} A_R & B_R \\ C_R & D_R \end{bmatrix}, \tag{4.14}$$

where elements of the matrix are

$$A_R = -\frac{f_A\left(\cos\left(gl_g\right)\right) - d_w g n_g \sin\left(gl_g\right)}{f_{tel}}, \tag{4.15}$$

$$\begin{aligned} B_R &= \left(\cos\left(gl_g\right) - d_w g n_g \sin\left(gl_g\right)\right) \\ &\times \left[f_A - \tfrac{f_{tel}(d_3 - f_A)}{f_A}\right] \frac{f_{tel}\left(\frac{\sin(gl_g)}{g} + n_g d_w \cos(gl_g)\right)}{f_A n_g}, \end{aligned} \tag{4.16}$$

$$C_R = \frac{f_A g n_g \sin\left(gl_g\right)}{f_{tel}}, \tag{4.17}$$

$$D_R = -\frac{f_{tel}\cos\left(gl_g\right)}{f_A} - g n_g \sin\left(gl_g\right)\left[f_A - \frac{f_{tel}\left(d_3 - f_A\right)}{f_A}\right]. \tag{4.18}$$

From the obtained relations, it is possible to calculate crucial parameters and make a design of the FPR.

4.3 Diffraction of the optical wave caused by Schmidt Cassegrain telescope

In FSO link, the receiver is irradiated by plane monochromatic wave with constant distribution of optical intensity. In our case the Schmidt Cassegrain telescope is used as a optical receiver system. This section deals with annular aperture diffraction caused by the circular aperture and secondary mirror obstruction of the Schmidt Cassegrain telescope. The central obstruction of the telescope affects the optical intensity distribution at the focal plane of the telescope. Because the light in fully photonic receiver is coupled to the optical fiber, one has to know to what extent the effect of diffraction on annular aperture influence the coupling efficiency of the Fully Photonic Link.

It is possible to say, that obscuration by the second mirror affect the diffraction pattern at the focal plane of the telescope. The practical effect of having a central obstruction in a telescope is that the central disc becomes slightly smaller, and the first bright ring becomes brighter at the expense of the central disc. This becomes more problematic with short focal length telescopes which require larger secondary mirrors.[22]

In order to find out the real diameter of the central diffraction disk, an experimental measurement was carried out. The Schmidt Cassegrain telescope was irradiated by a coherent optical plane wave. Using the interference on the plane–parallel plate the collimation of light incident on the Schmidt Cassegrain telescope was checked. The optical intensity at the focal plane of the telescope was recorded with a CCD beam profiler.

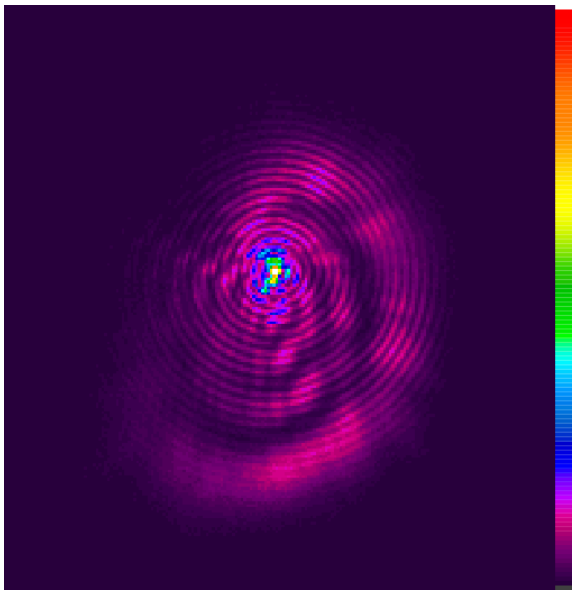

Fig. 4.4: Experimentally measured diffraction disk at the focal plane of the Schmidt Cassegrain telescope

The diffraction pattern at the focal point of the telescope is depicted in Fig. 4.4. The real radius of the central diffraction disc (white area in the center of the diffraction pattern) is around 20 μm which is very close to the theoretical expectations. The power contained in this area is much bigger than the power in the rest of the diffraction pattern.

In the case of FPR, the single mode optical fiber with collimating optics is placed to the center of the diffraction pattern when the maximum power is achieved. From a simple calculation, the coupling loss in the real scenario when the light from telescope is coupled into the SM fiber is around 6 dB. From Fig. 4.4, it is visible that some parasitic diffraction effects are present. The bigger diffraction rings are caused by diffraction of the optical wave on the central obstruction while the smaller diffraction rings are caused by the finite aperture of the telescope.

4.4 Testing Transmitter

For the estimation of the coupling efficiency of the FPR (free space to SM fiber), it was necessary to design the Testing Transmitter (TT). The TT should irradiate whole receiving aperture of the FPR under test.

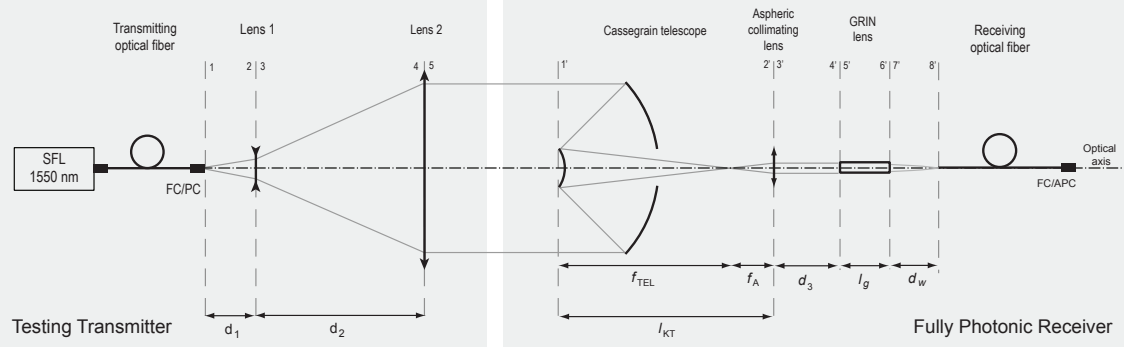

Fig. 4.5: Configuration of the testbed which consist of Testing Transmitter and Fully Photonic Receiver. SFL - Single Frequency Laser, Lens 1 - plano-concave lens with focal length $f_1 = -30\,mm$, Lens 2 - plano-convex lens with focal length $f_2 = 300\,mm$, f_{TEL} - focal length of the Cassegrain telescope, f_A - focal length of the aspheric collimating lens, l_g - length of the GRIN lens, d_w - working distance of the GRIN lens.

The Single Frequency laser in TT with wavelength of 1550 nm was used as a source and then it was coupled to the single-mode fiber with radius 5 μm. The sufficient irradiation of the receiver (FPR) aperture is ensured with beam expander which consist of two lenses Lens 1 and Lens 2 (Fig. 4.5). The design of the beam expander was carried out with geometrical optics. The transmitting optical fiber irradiates the Lens 1 from the distance d_1. This distance is represented by translation matrix

$$\mathbf{M_{12}} = \begin{bmatrix} 1 & d_1 \\ 0 & 1 \end{bmatrix}. \tag{4.19}$$

The Lens 1 was assumed as a thin lens with focal length f_1 with refraction matrix

$$\mathbf{M_{23}} = \begin{bmatrix} 1 & 0 \\ -1/f_1 & 1 \end{bmatrix}. \tag{4.20}$$

In order to collimate the wave emanating from the transmitting fiber the distance between the Lens 1 and Lens 2 is given by difference of the absolute value of their focal lengths

$$\mathbf{M_{34}} = \begin{bmatrix} 1 & d_2 \\ 0 & 1 \end{bmatrix}. \tag{4.21}$$

Then the Lens 2 was modelled as a refraction matrix of the thin lens with focal length f_2

$$\mathbf{M_{45}} = \begin{bmatrix} 1 & 0 \\ {}^{-1}/_{f_2} & 1 \end{bmatrix}. \tag{4.22}$$

The ray transfer matrix of the TT can be calculated as follows

$$\mathbf{M_T} = \mathbf{M_{45}} \cdot \mathbf{M_{34}} \cdot \mathbf{M_{23}} \cdot \mathbf{M_{12}}. \tag{4.23}$$

And finally the elements of the M_T

$$\mathbf{M_T} = \begin{bmatrix} A_T & B_T \\ C_T & D_T \end{bmatrix}, \tag{4.24}$$

are derived

$$A_T = 1 - \frac{d_2}{f_1}, \tag{4.25}$$

$$B_T = d_2 - \frac{d_1((d_2 - f_1)}{f_1}, \tag{4.26}$$

$$C_T = \frac{d_2 - f_1}{f_1 f_2} - \frac{1}{f_1}, \tag{4.27}$$

$$D_T = \frac{d_1\,(d_2 - f_2)}{f_1 f_2} - \frac{d_1 + d_2 - f_2}{f_2}. \tag{4.28}$$

From the ray transfer matrix the TT was set up in order to get collimated beam at the output.

4.5 Coupling efficiency

The complex envelope of a Gaussian beam is defined by the complex q parameter

$$\frac{1}{q(z)} = \frac{1}{R(z)} - j\frac{\lambda}{\pi w^2(z)}, \tag{4.29}$$

where $R(z)$ is the radius of the curvature and $w(z)$ is the radius of the beam waist. The properties of the optical system centered about the propagation axis can be described by the ray transfer matrix. Therefore the q_2 parameter of the Gaussian beam after the passage through an optical system can be deduced from an ABCD law as follows

$$q_2 = \frac{Aq_1 + B}{Cq_1 + D}, \tag{4.30}$$

where q_1 is the parameter of the input Gaussian beam and A, B, C, D are elements of the ray transfer matrix. After substitution of the Eq. (4.29) into the previous equation the radius of curvature and the beam waist radius can be derived as

$$R_2 = \frac{w_1^4\pi^2\left(A+\frac{B}{R_1}\right)^2 + B^2\lambda^2}{w_1^4\pi^2\left(A+\frac{B}{R_1}\right)\left(C+\frac{D}{R_1}\right) + BD\lambda^2}, \tag{4.31}$$

$$w_2 = \sqrt{\frac{w_1^4\pi^2\left(A+\frac{B}{R_1}\right)^2 + B^2\lambda^2}{w_1^2\pi^2\left(AD-BC\right)}}. \tag{4.32}$$

From these equations the q_2 parameter of the output Gaussian beam can be obtained.

In order to estimate the coupling efficiency of the optical receiver we used analytical Near-Field Method proposed by Kataoka [23]. The overlap integral characterizes the coupling efficiency between incident light and SM optical fiber [23]

$$\eta = \frac{|\int \psi_L\psi_F dr\ |^2}{\int |\ \psi_L\ |^2\ dr \int |\ \psi_F\ |^2\ dr}, \tag{4.33}$$

where ψ_L is relative field amplitude of the incident light and ψ_F is relative field amplitude of the optical fiber mode. It should be noted that the coupling efficiency expressed by equation (4.33) does not take into account any optical abberation. Equation (4.33) is only shown to be valid under assumption that the system is stationary and polarization independent and nonlinear effects does not occur. Optical fiber field amplitude is [23]

$$\psi_F = \sqrt{\frac{2}{\pi}}\frac{1}{w_F}\exp\left(-\frac{r^2}{w_F^2}\right), \tag{4.34}$$

where w_F is mode field radius of the fiber. We assume that the incident beam is a circularly symmetrical in terms of the radial coordinate r. Then the field amplitude of the incident light focused on the optical fiber is characterised as [23]

$$\psi_L = \sqrt{\frac{2}{\pi w_L^2}}\exp\left(-\frac{r^2}{w_L^2}\right), \tag{4.35}$$

where w_L is radius of the incident Gaussian beam. The coupling efficiency η is then defined as [23]

$$\eta(\Delta_x,\Delta_z) = \frac{4}{\left(\frac{w_F}{w_L}+\frac{w_L}{w_F}\right)^2 + \frac{\lambda^2\Delta_z^2}{\pi^2 w_F^2 w_L^2}}\exp -\frac{4\Delta_x^2}{w_F^2+w_L^2}, \tag{4.36}$$

$$\eta(\alpha) = \exp\left(-\frac{2\pi^2}{\lambda^2}\frac{\alpha^2 w_F^2 w_L^2}{(w_F^2+w_L^2)}\right), \tag{4.37}$$

where Δ_x is lateral deviation, Δ_z is defocus deviation and α is angular deviation of the receiving fiber (Fig. 4.6). Relation between FPR coupling efficiency and FPR coupling loss can be defined by expression

$$\alpha_{CL} = 10 \log \frac{1}{\eta}, \tag{4.38}$$

where α_{CL} is coupling loss in dB.

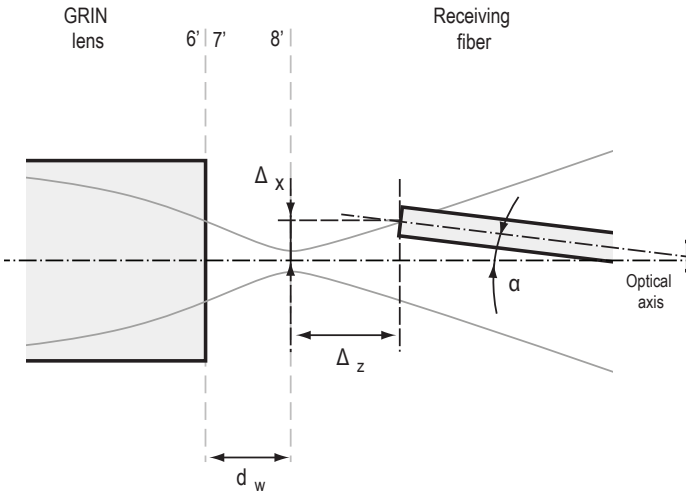

Fig. 4.6: Receiving fiber alignment deviations

Testbed parameters are listed in Table 4.1. The parameters of the Gaussian beam emanating from the transmitting fiber (at the plane 1) are w_1 and R_1. The beam waist of the Gaussian beam was placed exactly to back focal point of the Lens 1. From these parameters it is possible to obtain parameter q_1 from Eq. 4.29. We used the ray transfer matrices M_T and M_R in order to transform the q_1 into the q_2 parameter according to ABCD law (Eq. 4.30). Therefore we can calculate the parameters of the Gaussian beam behind the receiver at the plane 8'. The radius of curvature R_2 and beam radius w_2 of the transformed Gaussian beam was calculated from Eq. 4.31 and Eq. 4.32. The beam radius at the focus point of the GRIN lens is $w_2 = 17.4\,\mu m$ and the radius of curvature R_2 is infinite.

The FPR coupling efficiency was investigated for single-mode fiber with field radius $w_F = 4.5\,\mu m$. Once we know the field amplitude distribution of the optical fiber and incident light at the plane 8', we can estimate coupling efficiency from Eq. 4.36 and Eq. 4.37. The coupling loss in dB was determined according to Eq. 4.38. We obtained the coupling loss 5.2 dB for perfectly aligned system. To find out how the system will be sensitive to the alignment procedure, the coupling loss as a function of lateral deviation (Fig. 4.7a), angular deviation (Fig. 4.7b) and defocus deviation (Fig. 4.8) are depicted.

Tab. 4.1: Parameters of the testbed

TT parameters	
Wavelength λ	1550 nm
Beam waist radius w_1	4.5 μm
Radius of curvature R_1	∞
Focal length of the Lens 1 f_1	-30 mm
Focal length of the Lens 2 f_2	300 mm
Distance d_1	30 mm
FPR parameters	
Focal length of the Cassegrain telescope f_{tel}	1250 mm
Aperture radius of the Cass. telescope $D_{RXA}/2$	62.5 mm
Focal length of the aspheric lens f_A	4.51 mm
Distance d_3	1 mm
GRIN lens length l_g	4.43 mm
Gradient constant of the GRIN lens g	326 m^{-1}
Index of refraction at center of the GRIN lens n_g	1.5901
Working distance of the GRIN lens d_w	0.39 mm

According to these figures it is clear that alignment of the system is quite challenging, which indicates that some kind of adaptive technique should be used. For achievement of the sufficient power level the Erbium-doped Fiber Amplifier can be used conveniently.

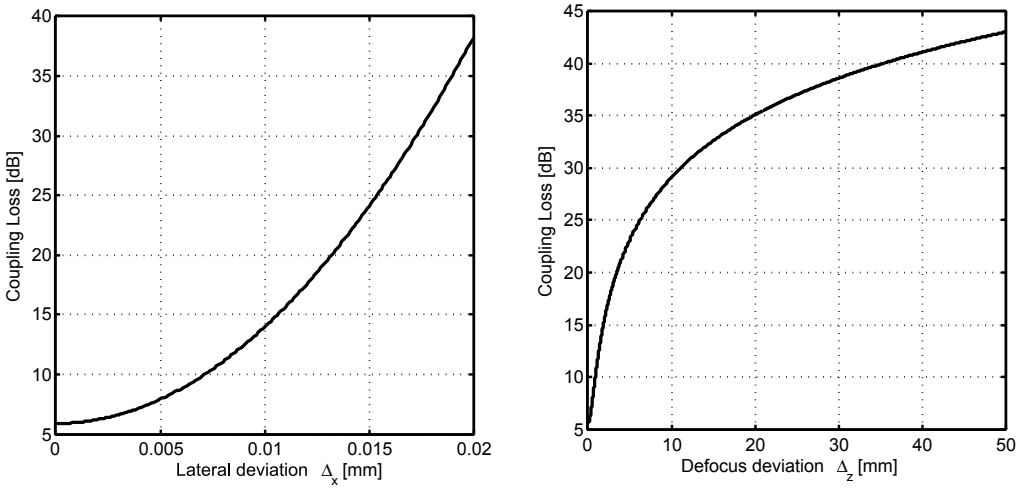

(a) The coupling loss of the FPR as a function of the lateral deviation

(b) The coupling loss of the FPR as a function of the defocus deviation

Fig. 4.7

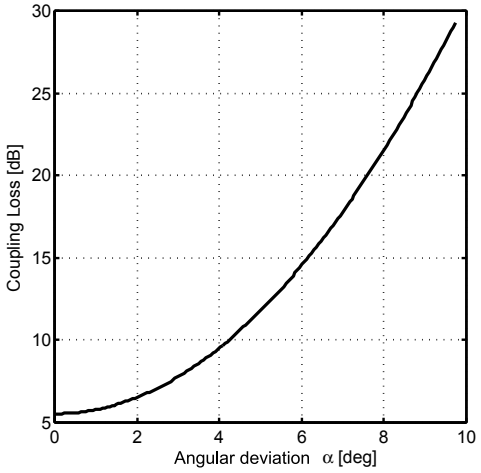

Fig. 4.8: The coupling loss of the FPR as a function of angular deviation.

4.6 Experimental measurement of the coupling loss

The system theoretically described in previous subsection was build up and tested. The testbed is depicted in Fig. 4.9. Construction elements from Thorlabs were used to build the system.

The coupling loss of the fully photonic receiver was measured for lateral and defocus deviation (Fig. 4.10a, 4.10b). Mechanical arrangement of the receiver does

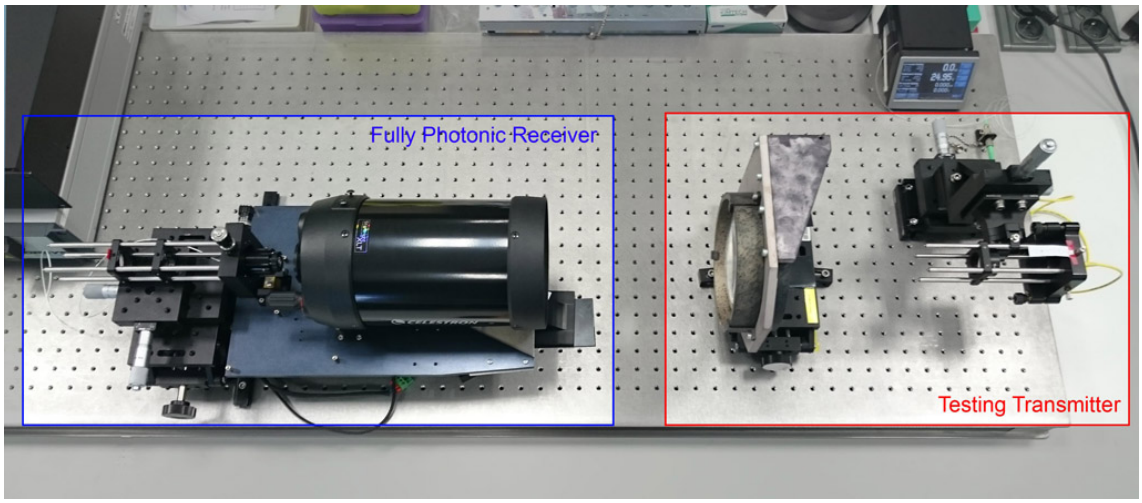

Fig. 4.9: Testbed for testing of the fully photonic receiver

not allow movement of the fiber tip. The GRIN element which is attached to the fiber and aspheric collimating lens are placed in one housing. Thus, we could move only with whole element instead of fiber. For this reason the measured values of the coupling loss are not the same. However, for the perfect alignment of the system the coupling loss is about 6 dB, which is close to the theoretical estimation.

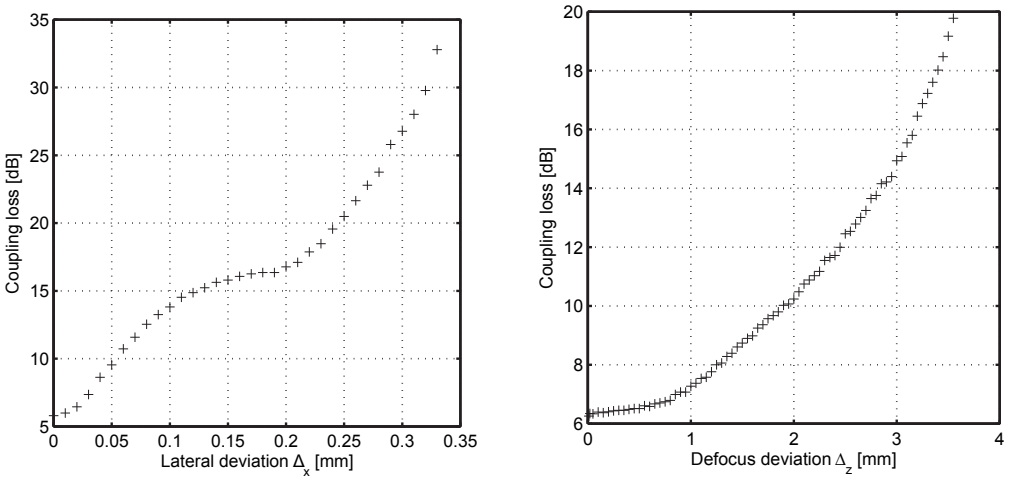

(a) The coupling loss of the FPR as a function of the lateral deviation.

(b) The coupling loss of the FPR as a function of the defocus deviation.

Fig. 4.10

4.7 Channel Characterization

A schematic concept of the fully photonic link is shown in Fig. 4.11. The input optical signal with wavelength 1550 nm is boosted in EDFA. The amplified signal (100 mW) is then led by single mode optical fiber to the transmitter, where large core fiber irradiates the transmitting lens. The optical Gaussian beam emanating from the transmitter ($D_{\mathrm{TXA}} = 50$ mm) has divergence $\theta = 1$ mrad. After propagation through the free space channel, the beam is received by the Schmidt-Cassegrain telescope (primary mirror diameter $D_{1,\mathrm{RXA}} = 125$ mm, secondary mirror diameter $D_{2,\mathrm{RXA}} = 50$ mm). The signal received by the Schmidt-Cassegrain telescope is then amplified by EDFA and filtered by a tunable fiber filter. The filtered optical signal is then distributed where it is needed. Example of possible energetic balance of the link was calculated in a special program which takes into account the statistical characteristics of the area. The results are shown in Tab. 4.2.

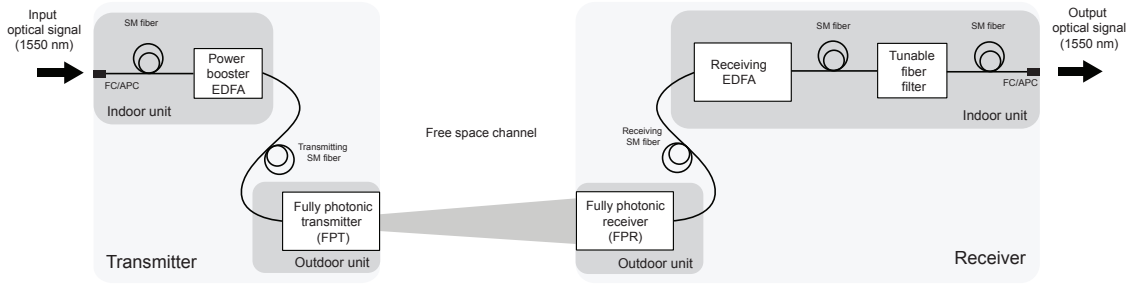

Fig. 4.11: Concept of the fully photonic link.

One of the effects caused by atmospheric turbulences, which have an essential impact on availability of the fully photonic link, is fluctuations of the angle of arrival. The incident angle is defined as the angle between the direction of propagation of an optical wave which is incident to the plane of the receiving aperture and optical axis of the receiver [24]. Fluctuations of angle of arrival have direct impact on coupling efficiency of a fully photonic link. As a consequence of angle of arrival fluctuation, the focused optical wave is shifted from the optical axis (image jitter) in the focal plane of the telescope. Due to this shift, the coupling loss increases.

The magnitude of angle of arrival fluctuation depends on the strength of the atmospheric turbulence. The strength of atmospheric turbulence is characterized by the refractive index structure parameter C_n^2. In the area of operation we expected values of the C_n^2 parameter between 10^{-13} m$^{-2/3}$ and 10^{-14} m$^{-2/3}$. It is assumed that the receiver will be placed at the far field; therefore we used relations for a spherical wave.

Transmitted optical power (mean)	$P_{\mathrm{m,TXA}}$	19.5	dBm
Beam divergence	θ	1	mrad
Link distance	L	850	m
Wavelength	λ	1550	nm
Transmitter system loss	$\alpha_{\mathrm{trans,\ syst}}$	5.5	dB
Atmospheric loss	α_{atm}	1	dB
Propagation loss	α_{prop}	37	dB
Diameter of receiving antenna (the primary mirror)	$D_{\mathrm{1,RXA}}$	125	mm
Diameter of receiving antenna (the secondary mirror)	$D_{\mathrm{1,RXA}}$	50	mm
Equivalent diameter of the (receiving antenna)	$D_{\mathrm{Eq,\ RXA}}$	114	mm
Total gain of the receiver	γ_{total}	17	dB
Received power	P_{RXA}	-7	dBm
Receiver system loss	$\alpha_{\mathrm{rec,\ syst}}$	15.5	dB
Receiver sensitivity (mean)	$P_{\mathrm{0,RXA}}$	-38	dBm
Margin of the link	M	15.5	dB

Tab. 4.2: Link budget.

After substituting of the link parameters (Tab. 4.2) we obtain variance of the angle of arrival approximately 8 μrad. Fluctuations of the angle of arrival in the focus plane of the telescope create an offset of the focus sometimes called "image jitter" or "image dancing". Owing to image jitter, the direction of propagation of light is changed at the input plane of the receiving fiber which causes coupling loss (α_{CL}).

The "image jitter" can be calculated as the root mean square angle of arrival multiplied by the focal length of the receiving telescope [25]. However, we have to take into account the whole receiving optical system including the collimating aspheric lens and GRIN lens. For this, we used relation (4.2) for estimating of the image displacement at the input plane of the receiving fiber. The value of image jitter is approximately 5 μm. From this value one can estimate the additional coupling loss caused by the angle of arrival from Fig. 4.7b. The loss is about 2 dB. For this particular application of the fully photonic link, the loss caused by the angle of arrival fluctuations is fully acceptable (see link margin in Tab. 4.2).

5 CONCLUSION

The doctoral thesis was focused on analysing the distribution of optical intensity within a laser beam at the transmitting aperture which is affected by propagation through free space as well as through the atmosphere. The aim of the thesis was to determine the optimal intensity distribution of the laser beam which is minimally affected by turbulence during the propagation. In the first part of the thesis the overall insight into the problem of Gaussian and Flattened Gaussian beam propagation through atmospheric turbulence was given. The numerical models of particular effects which influence beam quality are discussed. The various types of beam shapes were mentioned.

The numerical simulation of the arbitrary optical wave propagation through atmospheric turbulence was utilized and the results from the simulation were used in order to verify the theoretical models. From the theoretical analysis, it is assumed that the top-hat or Flattened Gaussian beam should have a lower scintillation index in comparison with the Gaussian beam. The simulation also showed that the aperture averaging effect has essential impact on scintillation reduction. Therefore the signal to noise ratio at the receiver increases.

Based on these findings, the available methods of beam shaping were studied. One of the options is using the plastic optical fiber as a beam shaper. For that case the optical intensity distribution of three different optical fibers was investigated. The output from the plastic optical fiber is created by thousand of modes whose envelope is similar to the Flattened Gaussian beam. Because the light emanating from the plastic optical fiber is partially coherent, the scintillation level could be reduced more.

The last chapter deals with modelling and designing a fully photonic link which will be used primarily for transmitting a highly stable optical frequency. The concept of a fully photonic transmitter was utilized. The optimal shape of the transmitted optical beam is ensured by a plastic optical fiber which irradiates the transmitting lens. The emanating optical beam has an optimal shape which is more resistant to the negative effects of atmospheric turbulence. The most challenging part of the fully photonic link is to design the fully photonic receiver. The aim of the receiver is to couple the light captured by the Schmidt Cassegrain telescope to the single mode optical fiber. The critical aspects which influence the coupling efficiency were discussed and modelled. The optical intensity distribution at the focal plane of the telescope and the effect of secondary mirror obscuration on resolving power was investigated by Fraunhofer diffraction. It was found that the obscuration by the secondary mirror improves the resolving power of the telescope which means that the central diffraction disk has a lower radius in comparison with a clear aperture.

However, less energy is included within the central diffraction disk. The fully photonic receiver coupling efficiency was estimated for a perfectly aligned system and for lateral, angular and defocus deviations. The modelled results were compared with experimental measurement on a testbed. Lastly the link budget and concept of the fully photonic link is given. The main contribution of this chapter is utilizing a fully photonic link with a beam shaper which is ready for experimental testing.

BIBLIOGRAPHY

[1] I. E. LEE, Z. GHASSEMLOOY, S. MEMBER, and W. P. NG, "Effects of Aperture Averaging and Beam Width on Gaussian Free Space Optical Links in the Presence of Atmospheric Turbulence and Pointing Error," in *14th International Conference on Transparent Optical Networks (ICTON), 2012*, 2012, pp. 2–5.

[2] P. KAUR, V. K. JAIN, and S. KAR, "Capacity of free space optical links with spatial diversity and aperture averaging," *2014 27th Biennial Symposium on Communications (QBSC)*, vol. 6, no. 3, pp. 14–18, Jun. 2014. [Online]. Available: http://ieeexplore.ieee.org/lpdocs/epic03/wrapper.htm?arnumber=6841175

[3] L. YANG, X. GAO, and M.S. ALOUINI, "Performance Analysis of Free-Space Optical Communication Systems With Multiuser Diversity Over Atmospheric Turbulence Channels," *IEEE Photonics Journal*, vol. 6, no. 2, pp. 1–17, Apr. 2014. [Online]. Available: http://ieeexplore.ieee.org/lpdocs/epic03/wrapper.htm?arnumber=6766188

[4] M.A. KHALIGHI, N. SCHWARTZ, N. AITAMER, and S. BOURENNANE, "Fading Reduction by Aperture Averaging and Spatial Diversity in Optical Wireless Systems," *Journal of Optical Communications and Networking*, vol. 1, no. 6, p. 580, Oct. 2009. [Online]. Available: http://www.opticsinfobase.org/abstract.cfm?URI=JOCN-1-6-580

[5] A. GARCIA-ZAMBRANA, C. CASTILLO-VAZQUEZ, and B. CASTILLO-VAZQUEZ, "Outage performance of MIMO FSO links over strong turbulence and misalignment fading channels." *Optics express*, vol. 19, no. 14, pp. 13 480–13 496, 2011.

[6] H. T. EYYBOGLU, Y. BAYKAL, E. SERMUTLU, O. KOROTKOVA, and Y. CAI, "Scintillation index of modified Bessel-Gaussian beams propagating in turbulent media." *Journal of the Optical Society of America. A, Optics, image*

science, and vision, vol. 26, no. 2, pp. 387–94, Feb. 2009. [Online]. Available: http://www.ncbi.nlm.nih.gov/pubmed/19183693

[7] H. T. EYYBOGLU, Y. BAYKAL, E. SERMUTLU, and Y. CAI, "Scintillation advantages of lowest order Bessel-Gaussian beams," *Applied Physics B: Lasers and Optics*, vol. 92, pp. 229–235, 2008.

[8] V. KOLLAROVA, T. MEDRIK, and R. CELECHOVSKY, "Application of nondiffracting beams to wireless optical communications," *Proc. SPIE*, 2007. [Online]. Available: http://www.opto.cz/tandem/publikace_pdf/%5B17%5D.pdf

[9] Y. CAI, "Propagation of various flat-topped beams in a turbulent atmosphere," *Journal of Optics A: Pure and Applied Optics*, vol. 8, no. 6, pp. 537–545, Jun. 2006. [Online]. Available: http://stacks.iop.org/1464-4258/8/i=6/a=008?key=crossref.d13f4016e37b776969a02269adef92a2

[10] M. ALAVINEJAD, B. GHAFARY, and F. KASHANI, "Analysis of the propagation of flat-topped beam with various beam orders through turbulent atmosphere," *Optics and Lasers in Engineering*, vol. 46, no. 1, pp. 1–5, Jan. 2008.

[11] H. T. EYYBOGLU, C. ARPALI, and Y. K. BAYKAL, "Flat topped beams and their characteristics in turbulent media." *Optics express*, vol. 14, no. 10, pp. 4196–207, May 2006.

[12] V. BAGINI, R. BORGHI, F. GORI, a. M. PACILEO, M. SANTARSIERO, D. AMBROSINI, and G. S. SPAGNOLO, "Propagation of axially symmetric flattened Gaussian beams," *Journal of the Optical Society of America A*, vol. 13, no. 7, p. 1385, Jul. 1996. [Online]. Available: http://www.opticsinfobase.org/abstract.cfm?URI=josaa-13-7-1385

[13] D. C. COWAN, J. RECOLONS, L. C. ANDREWS, and C. Y. YOUNG, "Propagation of flattened Gaussian beams in the atmosphere: a comparison of theory with a computer simulation model," in *Proc. of SPIE, Atmospheric Propagation III*, C. Y. Young and G. C. Gilbreath, Eds., vol. 6215, no. 1, May 2006, pp. 62 150B–62 150B–10.

[14] J. SCHMIDT, *Numerical Simulation of Optical Wave Propagation With Examples in MATLAB*. SPIE Press, 2010.

[15] F. M. DICKEY and S. C. HOLSWADE, *Laser Beam Shaping: Theory and Techniques*, ser. Optical Science and Engineering. Taylor & Francis, 2002.

[16] J. C. RICKLIN and F. M. DAVIDSON, "Atmospheric turbulence effects on a partially coherent Gaussian beam: implications for free-space laser communication." *Journal of the Optical Society of America. A, Optics, image science, and vision*, vol. 19, no. 9, pp. 1794–802, Sep. 2002. [Online]. Available: http://www.ncbi.nlm.nih.gov/pubmed/12216873

[17] Y. BAYKAL, H. T. EYYBOGLU, and Y. CAI, "Scintillations of partially coherent multiple Gaussian beams in turbulence." *Applied optics*, vol. 48, no. 10, pp. 1943–54, Apr. 2009. [Online]. Available: http://www.ncbi.nlm.nih.gov/pubmed/19340150

[18] M. PAVLU and J. POLIAK, "Modeling of the multichannel optical wireless link," in *Conference on Microwave Techniques (COMITE), 2013*, 2013, pp. 79–82.

[19] J. POLIAK, "Diffraction Effects in Transmitted Optical Beam," Doctoral thesis, Brno University of Technology, 2014.

[20] J. GERRARD, A. BURCH, *Introduction to Matrix Methods in Optics*, dover book ed. Dover, 1975.

[21] C. GOMEZ-REINO, M. V. PEREZ, C. BAO, and M. T. FLORES-ARIAS, "Design of GRIN optical components for coupling and interconnects," *Laser and Photonics Reviews*, vol. 2, no. 3, pp. 203–215, 2008.

[22] V. SACEK, "Notes on Amateur Telescope Optics," 2006. [Online]. Available: http://www.telescope-optics.net

[23] K. KATAOKA, "Estimation of coupling efficiency of optical fiber by far-field method," *Optical Review*, vol. 17, no. 5, pp. 476–480, 2010.

[24] L. C. ANDREWS and R. L. PHILIPS, *Laser Beam Propagation Through Random Media*, ser. Press Monographs. SPIE Press, 2005.

[25] L. C. ANDREWS, *Field Guide to Atmospheric Optics*. SPIE Press, 2004.

Peter Barcik

Technicka 3082/12
616 00 Brno
Czech Republic
Phone: +420 541 14 6558
E-mail: xbarci00@stud.feec.vutbr.cz

RESEARCH INTERESTS

Free space optical communication with special emphasis on atmospheric effects, modeling of laser beam propagation in turbulent media.

EDUCATION

since 2012 Brno University of Technology, Brno, Czech Republic

- Doctor of Philosophy (Ph.D.), Electronics and Communication
- Thesis: Analysis and optimalization of optical intensity distribution in a laser beam for optical wireless communication

2010 - 2012 Brno University of Technology, Brno, Czech Republic

- Master's degree (Ing.), Electronics and Communication
- Thesis: The distribution of relative variance of optical intensity in laser beam
- Deans award in 2012

2007 - 2010 Brno University of Technology, Brno, Czech Republic

- Bachelor's degree (Bc.), Electronics and Communication
- Thesis: Laboratory module of class D amplifier with PWM modulation

ACADEMIC APPOINTMENTS

- since 9/2012 Department of Radio Electronics, Brno University of Technology
- since 10/2012 Sensor, Information and Communications Systems (SIX) research group
- 10/2012 - 5/2014 Research assistant at Central European Institute of Technology (CEITEC)

RESEARCH STAY

- 1/2014 - 2/2014 Short Time Scientific Mission within COST IC1101 project
  Graz University of Technology, Austria
  Project: Modeling and Simulation of the Laser Beam Shaping Systems for FSO Terminal
  Supervised by: Prof. Erich Leitgeb

COMPUTER SKILLS

- Matlab - Intermediate
- OrCad PSpice, AutoCad, Eagle - Pre-Intermediate
- MS office, LaTeX - Advanced
- Adobe Creative Suite - Advanced
- Cinema 4D - Beginner

EXPERIENCE

- 07/2007 - 08/2007 LEONI Autokabel Slowakia, s.r.o., Ilava, Slovak Republic
- 07/2008 08/2008 Delta Electronics Slovakia, s.r.o., Dubnica nad Vahom, Slovak Republic

LANGUAGE SKILLS

- Slovak - Native speaker
- English - Intermediate
- Spanish - Basic knowledge
- German - Basic knowledge

ABSTRACT

The doctoral thesis is focused on analysing the distribution of optical intensity within a radiated laser beam at the plane of the transmitting (TXA) and receiving (RXA) aperture which is affected by propagation through free space as well as through the atmosphere. The aim of the thesis is to determine the optimal intensity distribution of the laser beam at the transmitter plane which is less affected by turbulence during propagation and transmitter aperture itself. In order to analyse the propagation of an optical wave through atmospheric turbulence, the simulation based on the Split-Step method is utilized. The propagation of the Flattened Gaussian beam was analysed for weak and moderate turbulence regimes. The thesis discusses usage of multimode fiber with large diameter as a shaping element and includes a design of the refraction beam shaper which is able to convert the Gaussian beam to a flattened Gaussian beam. Finally, a model of a fully photonic transmitter and receiver was built. The system is used for generating and receiving an optical coherent wave.

ABSTRAKT

Dizertačná práca je zameraná na štúdium a analýzu rozloženia optickej intenzity v laserovom zväzku v rovine vysielacej (TXA) a prijímacej apertúry (RXA), ktorý podlieha zmenám ako pri šírení voľným priestorom, tak pri šírení atmosférou. Cieľom práce je nájsť optimálne rozloženie optickej intezity v rovine vysielacej apertúry, ktoré bude minimálne ovplyvnené apertúrou vysielača a atmosférickými turbulenciami. Za účelom analýzy šírenia optickej vlny atmosférou bola využitá simulácia založená na metóde Split-Step. Šírenie Flattened Gaussian zväzku bolo analyzované pre režim slabých a stredných turbulencií. Práca sa zaoberá použitím multimódového vlákna s veľkým priemerom jadra ako tvarujúceho elementu a obsahuje návrh refrakčného tvarovača, pomocou ktorého je možno konvertovať Gaussovský zväzok na zväzok s uniformným rozložením optickej intenzity. Nakoniec je pomocou získaných poznatkov zostavený plne fotonický vysielač a prijímač, ktorých použitie spočíva v generovaní a príjmaní optickej koherentnej vlny prenášajúcej presnú fázu.

BARCÍK, Peter *Optimal intensity distribution in a laser beam for FSO communications*: short version of phd thesis. Brno: Brno University of Technology, Faculty of Electrical Engineering and Communication, Department of Radio Electronics, 2016. 37 p. Supervised by Prof. Ing. Otakar Wilfert, CSc.